A Novel Automatic Segmentation Method to Quantify the Effects of Spinal Cord Injury on Human Thigh Muscles and Adipose Tissue

Samineh Mesbah[1,2,5], Ahmed Shalaby[2], Sean Stills[4], Ahmed Soliman[2], Andrea Willhite[4,5], Susan Harkema[3,4,5], Enrico Rejc[3,4], and Ayman El-baz[2(✉)]

[1] Department of Electrical and Computer Engineering, University of Louisville, Louisville, KY, USA
[2] Department of Bioengineering, University of Louisville, Louisville, KY, USA
ayman.elbaz@louisville.edu
[3] Department of Neurological Surgery, University of Louisville, Louisville, KY, USA
[4] Kentucky Spinal Cord Injury Research Center, University of Louisville, Louisville, KY, USA
[5] Frazier Rehab Institute, Kentucky One Health, Louisville, KY, USA

Abstract. In this study, a novel automatic method for segmenting muscle groups and adipose tissue in thigh MRI volumes is developed to quantify the negative effects of spinal cord injury (SCI) on fat and muscle distribution in individuals with severe SCI. The thigh volumes were segmented based on subcutaneous fat, inter-muscular fat and muscle tissue using Linear Combination of Discrete Gaussians algorithm. Furthermore, the three main compartments of the muscle tissue: knee extensor, knee flexor and hip adductor muscles were segmented utilizing the Joint Markov Gibbs Random Field (MGRF) model that integrates first order appearance model of the muscles, spatial information, and shape model to localize the muscle groups. The method was tested on 10 SCI and 10 non-disabled (ND) subjects and the results has shown high accuracy of 96.86 ± 3.48 for fat segmentation and 94.76 ± 1.70 for muscle group segmentation based on Dice similarity percentage. Next, we calculated 3 ratios based on the volumes of the subcutaneous fat to muscle tissue, inter-muscular fat to muscle and extensor to flexor for all subjects. Mann-Whitney statistical test showed that inter-muscular fat to muscle ratio was significantly greater in SCI than in ND group (p = 0.001).

Keywords: MRI · LCDG · MGRF · Registration · Spinal cord injury

Electronic supplementary material The online version of this chapter (doi:10.1007/978-3-319-66185-8_79) contains supplementary material, which is available to authorized users.

M. Descoteaux et al. (Eds.): MICCAI 2017, Part II, LNCS 10434, pp. 703–711, 2017.
DOI: 10.1007/978-3-319-66185-8_79

1 Introduction

Magnetic resonance imaging (MRI) of thigh muscles is a commonly used technique to evaluate the effects of conditions such as ageing, obesity and spinal cord injuries (SCIs) on skeletal muscle mass and adipose tissue distribution [1, 2]. The volumetric thigh images that have been generated by 3D MRI are utilized to monitor the effectiveness of rehabilitation interventions and other treatments on reversing the negative physiological adaptations induced by these conditions on the skeletal muscle system. In order to find quantification measures for [3] evaluation and comparison, the MRI volumes must first be segmented based on muscle tissue, subcutaneous fat and inter-muscular fat. It is also of importance to assess and compare the muscle mass of specific muscle groups or individual muscles.

The task of segmenting MR images into meaningful compartments has usually been done manually by experts. However, the manual methods have been suffering from inter- and intra-operator variability, being laborious and time-consuming and hence not being scalable to a higher number of patients and treatment methods. Therefore, reliable and accurate automatic or semi-automatic methods for detecting anatomical volumes of interest from MR images are highly needed and will offer reliability, repeatability and scalability in various medical applications.

Several automatic and semi-automatic methods have been proposed in the literature for segmentation of thigh MR images. Positano et al. [4] used a fuzzy clustering technique and an active contour algorithm to segment the subcutaneous fat and bone in thigh MR images recorded from obese individuals. They also used an expectation maximization (EM) algorithm to segment the inter-muscular fat from soft tissue. In a similar study, Urricelqui et al. [5] used an intensity-based method with adaptive thresholding for segmenting bone, fat tissue and muscle tissue. Makrogiannis et al. [6] used parametric deformable model to segment subcutaneous fat and central clustering technique to identify the inter-muscle fat from muscle tissue. An unsupervised multi-parametric k-means clustering method proposed in [7] to segment inter-muscular, subcutaneous fat and muscle tissue in patients with type 2 diabetes and in the control group. Moreover, Orgiu et al. [8] used a fuzzy c-mean algorithm and Snake active contour model to distinguish between inter-muscular and subcutaneous fat in obese and elderly individuals (also see [9]).

All of these studies are focused on segmentation of fat and muscle area in 2-D images using intensity and shape-based methods only. However, no muscle group segmentation was done in these studies. There have been a number of studies done recently on muscle volume segmentation on 3-D MRI datasets of thigh muscles where the objective was to segment the entire volume of certain muscle groups or each individual muscle in addition to subcutaneous and inter-muscular fat segmentation. Baudin et al. [3] presented a method for encoding shape models based on training dataset into a random walker segmentation framework to segment each individual muscle of the human thigh. In a similarly task, Andrews and Hamarneh [10] proposed a probabilistic approach to build a statistical shape model using the principal component analysis to a set of M K-label manually generated training segmentations. Ahmad et al. [11] proposed a combination framework of atlas construction and image registration to

segment the quadriceps muscle group. However, no segmentation of adipose tissue was done in this study. Another atlas-based segmentation method was proposed by Le Troter et al. [12] to segment four individual muscle volumes inside the quadriceps group. They presented single-atlas and multiple-atlas approaches for the segmentation, suggested that the single-atlas method was more robust for single muscle segmentation and has a better accuracy. However, there is no utilization of any appearance features in their model and they only focused on young healthy male population, which as mentioned in [8] some of the proposed automatic methods for segmentation might show poor accuracy in populations with medical conditions that negatively affect the muscle and fat infiltration areas. Furthermore, none of the aforementioned studies focused on using automatic segmentation methods on severe SCI population.

In this paper, we introduce a new automatic technique to quantify the negative effects of severe SCI on thigh muscles and fat distribution in humans. In SCI individuals, the muscle paralyzed by an upper motor neuron lesion undergoes severe atrophy and consequently the reduction of force generation capability. These negative adaptations, among others, may limit motor functions even if neuronal control was sufficient. These individuals are also prone to gain adipose tissue at different sites (i.e. subcutaneous and inter-muscular fat), which can also lead to secondary complications such as higher risk of diabetes, cardiovascular diseases and metabolic syndrome [13]. We propose a computer-based approach to (1) automatically segment MRI volumes of adipose tissue into subcutaneous and inter-muscular fat using an intensity-based approach; (2) segment the MRI volumes related to the thigh muscle tissue into three main muscle groups: knee extensors, knee flexors and hip adductor muscles using the joint Markov Gibbs Random Field (MGRF) model. The main motivation behind developing the joint MGRF model is to use intensity, spatial and shape concurrently to overcome intensity-based variations, handle the intra-/inter-muscle inhomogeneity and define muscle compartments, respectively.

Prior to presenting the proposed method, we will define some basic terminologies, as in [14]. Let $\mathbf{R} = \{(x, y, z) : 0 \leq x \leq X - 1, 0 \leq y \leq Y - 1, 0 \leq z \leq Z - 1\}$; $\mathbf{Q} = \{0, 1, \ldots, Q - 1\}$; and $\mathbf{L} = \{0, 1, 2, 3\}$ denote a finite 3-D arithmetic lattice of the size of XYZ supporting grayscale images and their region (segmentation) maps, a finite set of Q integer gray values, and a set of region labels, respectively. Let $\mathbf{g} = \left\{g_{x,y,z} : (x, y, z) \in \mathbf{R}; g_{x,y,z} \in \mathbf{Q}\right\}$ and $\mathbf{m} = \left\{m_{x,y,z} : (x, y, z) \in \mathbf{R}; m_{x,y,z} \in \mathbf{L}\right\}$ be a grayscale image taking values from $\mathbf{Q}$, i.e., $\mathbf{g} : \mathbf{R} \rightarrow \mathbf{Q}$, and a region map taking values from $\mathbf{L}$, i.e., $\mathbf{m} : \mathbf{R} \rightarrow \mathbf{L}$, respectively.

2 Methods

A 3-D probabilistic based framework for fat suppressed (FS) and water suppressed (WS) MRI muscles and fat segmentation is proposed in Fig. 1. The proposed system consists of the following four steps: (1) As a preprocessing step, the sum of WS and FS volumetric MRI is utilized to get the mask of the whole thigh volume utilizing Linear Combination of Discrete Gaussians (LCDG) algorithm [14]. Same method was used on each FS-MRI volume to initially extract muscle volume and WS-MRI volume is used

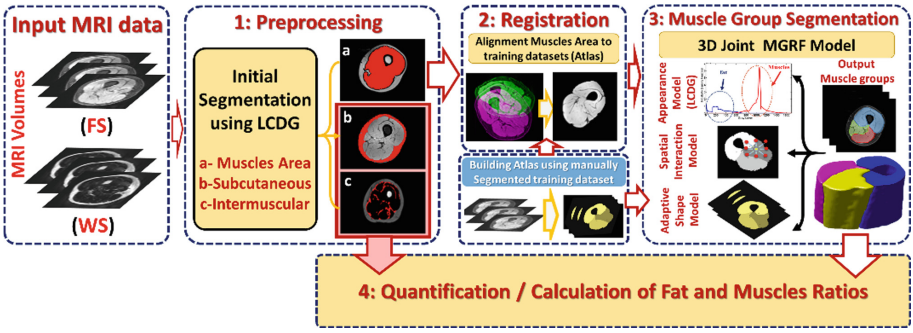

Fig. 1. The proposed framework for muscles/fat analysis based on MRI data.

to segment the total adipose tissue and bone. Moreover, the subcutaneous fat was separated from the inter-muscular fat by overlaying the muscle tissue mask, obtained from the FS volume, on the total fat segmentation; (2) Each segmented muscle volume and its manually segmented muscle groups (training dataset) is co-aligned to a reference dataset using a 3-D cubic B-splines-based approach (described in [15]) to account for the anatomical differences of each patient's extracted muscle volumes from adipose tissue and bone; (3) Implementing a joint MGRF model that simultaneously maximizes the likelihood estimation of three components: Appearance-based shape (muscles anatomy), spatial (second order appearance) and intensity (first order appearance) model by using iterated conditional modes (ICM) to segment/localize the three muscle groups: knee extensors, knee flexors and hip adductors for the test subjects; and (4) Quantifying the effects of SCI on human thigh muscles by calculating fat to muscle ratios.

Details of the joint MGRF model and its sub-components are outlined below.

2.1 Joint Markov Gibbs Random Field Model

In order to divide the extracted muscles area into various groups, a registered-to-reference database of grayscale volume, $\mathbf{g}$, of the muscles area and its map, $\mathbf{m}$, are described with a joint probability model: $P(\mathbf{g},\mathbf{m}) = P(\mathbf{g}|\mathbf{m})P(\mathbf{m})$, which combines a conditional distribution of the input volume given the map $P(\mathbf{g}|\mathbf{m})$, and an unconditional probability distribution of maps $P(\mathbf{m}) = P_{sp}(\mathbf{m})P_{\mathbf{V}}(\mathbf{m})$, where, $P_{sp}(\mathbf{m})$ represents an adaptive shape prior. $P_{\mathbf{V}}(\mathbf{m})$ is a Gibbs probability distribution with potentials $\mathbf{V}$, which denotes a sample of a 3D MGRF model of $\mathbf{m}$ [16].

2.2 Appearance-Based Shape Model

In order to reduce the variability across subjects and enhance the segmentation accuracy, an adaptive shape model of each muscle group is employed. To create the shape database, a training set of volumes, collected from different subjects, are registered to a reference dataset using a 3-D B-splines-based transformation developed in [15].

The probabilistic shape priors are spatially variant independent random fields of region labels, as follows:

$$P_{sp}(\boldsymbol{m}) = \prod p_{sp:x,y,z}(m_{x,y,z}) \tag{1}$$

where $p_{\mathrm{sp}:x,y,z}(l)$ is the voxel-wise empirical probabilities for each label $l \in \mathbf{L}$. To segment each input MRI data, an adaptive process guided by the visual appearance features of the input MRI data is used to construct the shape prior. This shape prior consists of four labels: the 3 muscle groups and the background. In the training phase, we use N-1 (N number of subjects) manually segmented data sets by an MRI expert to create the probabilistic maps for the four labels. For the testing phase, each test MRI volume is registered using the same approach in [15], to the training sets used to create the discussed shape prior.

2.3 Spatial Interaction or Second-Order Appearance Model

In order to overcome noise effects and to ensure segmentation homogeneity, spatially homogeneous 3D pair-wise interactions between the region labels are additionally incorporated in the proposed segmentation model. These interactions are estimated using the Potts model, i.e., an MGRF with the nearest 26-neighbors of the voxels (also known as cliques), and analytic bi-valued Gibbs potentials, that depend only on whether the nearest pairs of labels are equal or not. The utilized second-order 3D MGRF model of the region map $\mathbf{m}$ is defined as:

$$P_V(\mathbf{m}) = \frac{1}{Z_{v_s}} \exp \sum\nolimits_{(x,y,z)\in \boldsymbol{R}} \sum\nolimits_{(x',y',z')\in v_s} \mathrm{V}\left(\mathbf{m}_{x,y,z}, \mathbf{m}_{x+x',y+y',z+z'}\right), \tag{2}$$

where Z_{v_s} is the normalization factor. Let $f_{\mathrm{eq}}(\mathbf{m})$ denote the relative frequency of equal labels in the neighboring voxel pairs. The initial region map results in an approximation with the following analytical maximum likelihood estimates of the potentials [17]:

$$v_{\mathrm{eq}} = -v_{\mathrm{ne}} \approx 2f_{\mathrm{eq}}(\mathbf{m}) - 1, \tag{3}$$

which allows for computing the voxel-wise probabilities $p_{\mathbf{V}:x,y,z}(l)$ of each label; $l \in \mathbf{L}$. More details are in [14].

2.4 Intensity or First-Order Appearance Model

Our approach also accounts for the visual appearance of the muscles besides the learned shape model and the spatial interactions, therefore, an intensity-based model using LCDG with positive and negative components, is applied to improve the refinement speed as well as increasing the initially obtained accuracy. The role of LCDG is to accurately approximate the empirical gray level distribution of FS-MRI voxel intensities to two distinct components associated with each label [14]. This approximation adapts the segmentation to the changing appearance, such as non-linear

intensity variations caused by data acquisition systems. At the end of this stage, each grayscale voxel existed in the target volume was initially mapped to a class with the highest occurrence probability. The muscles group segmentation procedure is summarized in Algorithm 1 at the supplementary materials.

3 Experimental Results

The 3-D MRI slices were recorded using Siemens 3T Magnetom Skyra with pulse sequence – t1 vibe (for 3-D VIBE images) for in phase, opposite phase, water, and fat imaging. The volume dimensions (X, Z, Y) are 320 × 320 × 208 and the series length is 1. Voxel dimensions (X, Z, Y) are 1.5 × 1.5 × 1.5 mm, size of series point is 0.006 s and the slice gap is equal to zero. The thigh MRI scans analyzed in this study (N = 20) were collected from 10 male individuals with chronic motor complete SCI (age: 34.4 ± 9.0 years; time since injury: 7.3 ± 8.9 years; 7 of them with American Spinal Injury Association Impairment Scale (ASIA) score A, 2 with score B and 1 with score C) and 10 healthy male non-disabled subjects (age 28.7 ± 3.8). All participants were fully informed about the aim of the study and have provided their written consents, which have been approved by the University of Louisville Institutional Review Board.

In this study, the 50 central MRI slices between greater trochanter and lateral epicondyle of the femur were considered for further analysis. All manual segmentations used in training and verifying the segmentation results were created and revised by MRI experts using MANGO software.

Figure 2 shows an example of the LCDG results on the FS- and WS-MRI volumes for extraction of the whole muscle area, bone, and segmenting the subcutaneous fat from the inter-muscular fat. In Fig. 3 the three steps for muscle groups segmentation is presented for four sample MR images.

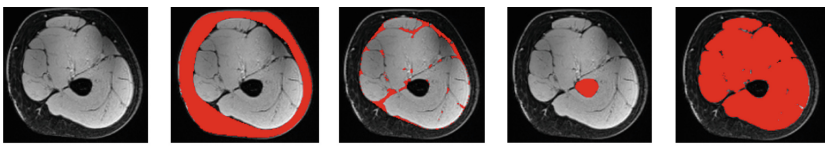

Fig. 2. Examples for the utilization of LCDG to segment the soft tissue: (a) original image; Red area shows: (b) subcutaneous fat, (c) inter-muscular fat, (d) bone, and (e) muscle area.

The accuracy of the initial segmentation of fat tissue was tested by comparison of the automatic results with the manual segmentation of subcutaneous and inter-muscular fat. The comparison was made based on calculating the Dice similarity coefficient (DSC) as the similarity measure. To obtain the accuracy for automatic muscle groups segmentation, we used the common technique of leave-one-subject-out, where N−1 subjects are used to build the atlas and one subject was left out for testing, and repeat this for all subjects for SCI and ND groups separately. The results for accuracy measures are presented in Table 1.

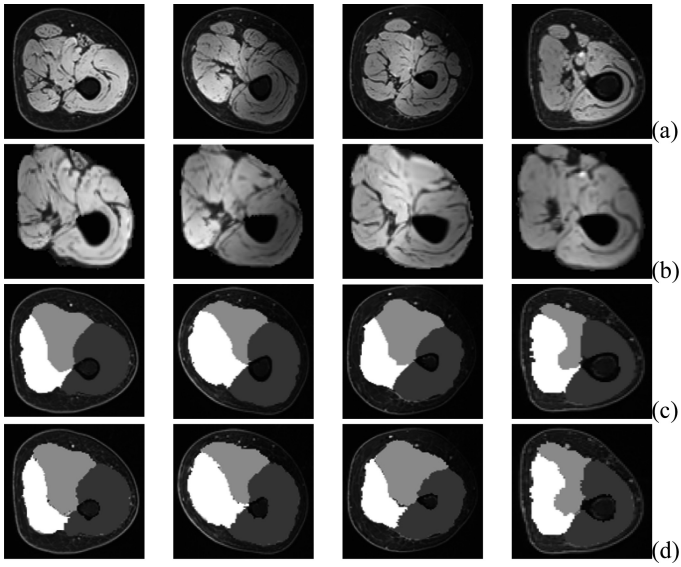

Fig. 3. Four Examples of muscle group segmentation algorithm: (a) original image, (b) registration to the reference atlas, (c) manually segmented muscle groups, and (d) automatic segmentation of muscle groups.

Table 1. The accuracy measure (percentage of DSC) of the proposed approach for 10 SCIs and 10 NDs

SCI IDs	1	2	3	4	5	6	7	8	9	10
Muscle group segmentation	93.56	91.17	94.50	93.69	93.99	94.24	95.01	91.10	93.64	94.53
Total fat segmentation	98.30	94.84	99.69	99.58	95.78	98.77	93.20	86.34	93.95	95.38
ND IDs	1	2	3	4	5	6	7	8	9	10
Muscle group segmentation	96.52	95.26	96.54	96.46	96.42	94.68	95.62	94.16	97.06	97.16
Total fat segmentation	98.71	95.97	98.34	98.75	99.94	99.60	99.68	98.43	92.07	99.81

Finally, the three ratios based on the volumes of the subcutaneous fat to muscle tissue, inter-muscular fat to muscle and extensor to flexor for all subjects in SCI and ND groups were calculated (Fig. 4). In order to see if there is a statistically significant difference between SCI and ND groups, we used the non-parametric Mann-Whitney test on the three ratios and results show that the inter-muscular fat to muscle volume shows significant difference between the two groups (2-tailed $p = 0.001$)

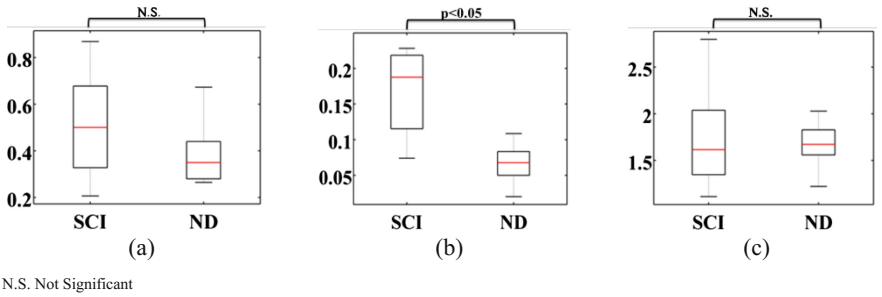

Fig. 4. The boxplot representation of the calculated ratios: (a) subcutaneous volume/Muscle volume, (b) inter-muscular volume/muscle volume, and (c) extensor volume/flexor volume

4 Conclusions

An automatic framework was proposed to precisely segment thigh muscle groups and fat volumes in healthy and SCI individuals with total accuracy of 94.76±1.70 for muscle group segmentation and 96.86 ± 3.48 for total fat segmentation. The high accuracy presented in the results section for muscle group segmentation demonstrates the advantage of incorporating appearance and spatial information into a level-set model for automatic muscle volume segmentation. While the main focus of this study was on SCI subjects, the close accuracy in the ND group supports the claim that our proposed framework has the capacity to be applied in broad population where the segmentation of thigh muscle and fat volumes can be a valuable assessment. The proposed framework is able to accurately segment and compartmentalize muscle and adipose tissue, and detect changes within a compartment. In this case, it was able to demonstrate an increase in inter-muscular fat relative to muscle volume in patients with SCI. There is a promise that this methodology could have broad application in detecting, and tracking over time, muscle atrophy in patients with loss of mobility and muscle mass gain due to rehabilitative interventions.

References

1. Elder, C., Apple, D., Bickel, C., Meyer, R., Dudley, G.: Intramuscular fat and glucose tolerance after spinal cord injury – a cross-sectional study. Spinal Cord **42**, 711–716 (2004)
2. Pisot, R., Marusic, U., Biolo, G., Mazzucco, S., Lazzer, S., Grassi, B., Reggiani, C., Toniolo, L., di Prampero, P., Passaro, A., Narici, M., Mohammed, S., Rittweger, J., Gasparini, M., Gabrijelčič Blenkuš, M., Šimunič, B.: Greater loss in muscle mass and function but smaller metabolic alterations in older compared to younger men following two weeks of bed rest and recovery. J. Appl. Physiol. **120**, 922–929 (2016)
3. Baudin, P., Azzabou, N., Carlier, P., Paragios, N.: Prior knowledge, random walks and human skeletal muscle segmentation. In: MICCAI, pp. 569–576 (2012)
4. Positano, V., Christiansen, T., Santarelli, M., Ringgaard, S., Landini, L., Gastaldelli, A.: Accurate segmentation of subcutaneous and intermuscular adipose tissue from MR images of the thigh. J. Magn. Reson. Imaging **29**, 677–684 (2009)

5. Urricelqui, L., Malanda, A., Villanueva, A.: Automatic segmentation of thigh magnetic resonance images. International Journal of Medical, Health, Biomedical, Bioengineering and Pharmaceutical Engineering **3**(10), 314–320 (2009)
6. Makrogiannis, S., Serai, S., Fishbein, K., Schreiber, C., Ferrucci, L., Spencer, R.: Automated quantification of muscle and fat in the thigh from water-, fat-and non-suppressed MR images. J. Magn. Reson. Imaging **35**(5), 1152–1161 (2012)
7. Valentinitsch, A., Karampinos, D., Alizai, H., Subburaj, K., Kumar, D., Link, T., Majumdar, S.: Automated unsupervised multi-parametric classification of adipose tissue depots in skeletal muscle. J. Magn. Reson. Imaging **37**(4), 917–927 (2013)
8. Orgiu, S., Lafortuna, C., Rastelli, F., Cadioli, M., Falini, A., Rizzo, G.: Automatic Muscle and fat segmentation in the thigh from T1-weighted MRI. J. Magn. Reson. Imaging **43**(3), 601–610 (2015)
9. Tan, C., Yan, Z., Yang, D., Li, K., Yu, H., Engelke, K., Miller, C., Metaxas, D.: Accurate thigh inter-muscular adipose quantification using a data-driven and sparsity-constrained deformable model. In: IEEE ISBI, NYC, pp. 1130–1134 (2015)
10. Andrews, S., Hamarneh, G.: The generalized log-ratio transformation: learning shape and adjacency priors for simultaneous thigh muscle segmentation. IEEE Trans. Med. Imaging **34** (9), 1773–1787 (2015)
11. Ahmad, E., Yapa, M., Degensb, H., McPhee, J.: Atlas-registration based image segmentation of MRI human thigh muscle in 3-D space. In: Proceedings of SPIE (2014)
12. Le Troter, A., Fouré, A., Guye, M., Confort-Gouny, S., Mattei, J., Gondin, J., Salort-Campana, E., Bendahan, D.: Volume measurements of individual muscles in human quadriceps femoris using atlas–based segmentation approaches. J Magn. Reson. Mater. Phys. **29**, 245–257 (2016)
13. Gorgey, A., Dolbow, D., Dolbow, J., Khalil, R., Castillo, C., Gater, D.: Effects of spinal cord injury on body composition and metabolic profile – Part I. J. Spinal Cord Med. **37**, 693–702 (2014)
14. Farag, A., El-baz, A., Gimelfarb, G.: Precise segmentation of multi-modal images. IEEE Trans. Image Process. **15**(4), 952–968 (2006)
15. Glocker, B., Sotiras, A., Komodakis, N., Paragois, N.: Deformable medical image registration: Setting the state of the art with discrete methods. Ann. Rev. Biomed. Eng. **13**, 219–244 (2011)
16. El-Baz, A., Gimel'farb, G., Suri, J.: Stochastic Modeling for Medical Image Analysis. Taylor & Francis, Abingdon (2016)
17. Khalifa, F., Beache, G., Gimel'farb, G., Giridharan, G., El-Baz, A.: Accurate automatic analysis of cardiac cine images. IEEE Trans. Biomed. Eng. **59**(2), 445–455 (2012)